THE JOURNAL OF PHYSICAL CHEMISTRY C

Article

Cite This: J. Phys. Chem. C 2018, 122, 24190−24201

pubs.acs.org/JPCC

Structure and Vibrational Properties of Potassium-Promoted Tungsten Oxide Catalyst Monomeric Sites Supported on Alumina ($K_2O/WO_3/Al_2O_3$) Characterized Using Periodic Density Functional Theory

Daniyal Kiani,[†] Gustavo Belletti,[‡] Paola Quaino,[‡] Frederik Tielens,*[,§] and Jonas Baltrusaitis*[,†]

[†]Department of Chemical and Biomolecular Engineering, Lehigh University, B336 Iacocca Hall, 111 Research Drive, Bethlehem, Pennsylvania 18015, United States

[‡]Instituto de Química Aplicada del Litoral, IQAL (UNL-CONICET), PRELINE (FIQ-UNL), Universidad Nacional del Litoral, S2829 Santa Fe, Argentina

[§]General Chemistry (ALGC), Vrije Universiteit Brussel (Free University Brussels-VUB), Pleinlaan 2, 1050 Brussel, Belgium

ABSTRACT: Al_2O_3-supported tungsten oxide catalysts have been instrumental in many industrially relevant reactions and their reactivity is controlled by their molecular structure. In turn, their molecular structure has primarily been derived via Raman measurements with assignments made using model compounds of known local (molecular) coordination. In this work, the structure and simulated Raman spectra of unpromoted and K^+-promoted tungsten oxide catalyst monomeric sites supported on γ-Al_2O_3(110) ($K_2O/WO_x/\gamma$-Al_2O_3(110)) were studied using periodic DFT methods. Two different WO_x-grafted monomers on the γ-Al_2O_3(110) surface were identified with a total energy difference of 0.17 eV between both structures. Importantly, both structures showed the presence of W═O and W−OH moieties, thus providing additional insights into experimental Raman data, which typically describe only W═O moieties. The grafted WO_3 species were stabilized when the present W−OH groups were oriented toward the alumina surface leading to the formation of H-bonds, calculated at 1039 cm^{-1}, for example in the vicinity of the W═O vibrations. The W═O bond length was altered in the presence of K^+, as shown experimentally and theoretically in blue shifting of the Raman band corresponding to W═O. The W vibrations were well localized in the calculated spectra, and little shifts were observed upon the different WO_x molecular geometry, explaining why a single Raman peak is mostly observed experimentally. The acidity of the lowest energy catalyst structures was investigated by simulated NH_3 adsorption vibrational frequency and binding energy calculations. Results suggested that NH_3 prefers to bind in a Lewis-like structure with no proton donation from either W−OH or Al−OH moiety. This challenged some of the literature observations where Brønsted acid sites have been suggested to exist on near-monolayer coverage WO_x species on γ-Al_2O_3 prepared by calcining at moderate (400 °C) to high temperatures (700 °C). Overall, this work provided new insights into the molecular structure of WO_x/γ-Al_2O_3 and $K_2O/WO_x/\gamma$-Al_2O_3 catalysts not immediately available from experimental measurements alone.

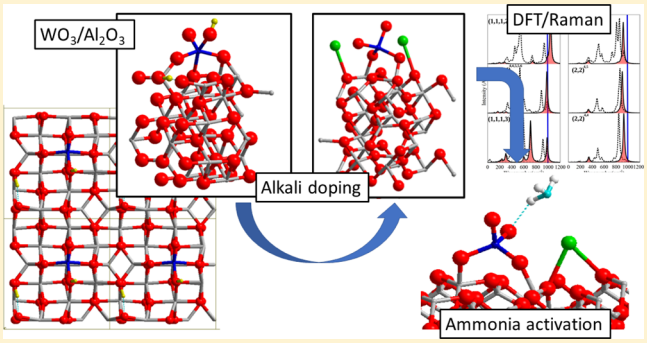

INTRODUCTION

Supported transition metal oxides are among the most important catalytic systems used today.[1] Metal and metalloid oxide-supported WO_3 catalysts have been utilized in numerous chemical industrial and environmental processes including alkane isomerization,[2−4] alcohol dehydration, dehydrogenation and condensation,[3,5−7] hydrodesulfurization,[8] metathesis,[9−11] selective catalytic reduction,[12] and CO_2[13] and hydrocarbon hydrogenation reactions.[14] Of significant importance to the chemicals industry is also the catalytic reactions of sulfur-containing gas molecules with these supported transition metal oxide (or their corresponding sulfide)[15−18] catalysts, such as WO_3 and K^+-promoted WO_3.[6,13,19,20] While the former rely mostly on the ability to synthesize tungsten oxide sites of well-defined acid strength and density, the latter rely on a complete restructuring of the catalytic sites to yield sulfur derived surface species, such as those formed by dissociation of H_2S on the Lewis sites.[15] An interesting observation related to the stoichiometry of the promoter (K_2O) and catalyst WO_3 material emerged, where CH_3SH formation from $CO/H_2/H_2S$ and $CO_2/H_2/H_2S$ mixtures on $K_2O/WO_3/Al_2O_3$ showed greatest selectivity toward the product at W/K ratio corresponding to the stoichiometric K_2WO_4.[13] For this reason, the succeeding studies prepared CH_3SH catalysts directly using

Received: August 23, 2018
Revised: October 1, 2018
Published: October 3, 2018

DOI: 10.1021/acs.jpcc.8b08214
J. Phys. Chem. C 2018, 122, 24190−24201

aqueous K_2WO_4 solution via impregnation of Al_2O_3.[17,18] Different groups have investigated the role of the support in this catalyst, and the most commonly studied supports are silica,[21] alumina,[21,22] zirconia,[21,23] and titania[24]—partly owing to their specific physicochemical properties and partly to their abundance and relatively low prices.[25] Interestingly, K_2WO_4 emerged to be the common active material in most cases, suggesting a particular catalyst structure leading to enhanced catalytic properties. Computationally, such small, isolated K and W-containing structures can be modeled to gain some understanding regarding their structures and effects on the catalytic material. Molecular structures of these K and W-containing catalysts as well as the resulting structure−property relationships are hence of fundamental importance.

In a supported transition metal oxide catalyst, the two most important parameters that control the catalytic performance are as follows. The first parameter is the nature and structure of the surface species, for example, the active sites present on the surface of the support as they can be acidic or basic, either Lewis and Brønsted, which affects the overall catalytic mechanism. The molecular geometry of the active site is of importance, as different molecular geometries of the active site exhibit different catalytic properties. In general, these supported metal oxide species on the surface can be isolated, oligomeric, semipolymeric, or fully polymeric, which further has implications on the mechanism that the catalytic process proceeds.[21,26−28] The second parameter is the active metal oxide coverage, where the maximum amount of metal oxide that can be anchored on the support in a two-dimensional fashion catalyst affects the overall activity.[27] WO_3 supported on γ-Al_2O_3 exhibits strong interaction with the support leading to observable changes in the properties of both tungsten oxide and alumina. For example, supported WO_3 inhibits transformation of γ-Al_2O_3 into α-Al_2O_3, normally taking place via condensation of hydroxyl groups and elimination of H_2O.[22] This is due to the fact that WO_3 species bond to the surface via the condensation of the hydroxyl groups.[22,29] Direct reaction between WO_3 and Al_2O_3 has only been experimentally observed at high temperatures of ∼1150 °C, when the tungsten oxide coverage is at or below the monolayer (1 ML = ∼4.3 W atoms/nm^2). At high coverages (∼3 × ML), the reaction between WO_3 and Al_2O_3 was observed even at ∼500 °C. It was reasoned that until monolayer coverage a virtually irreducible and highly dispersed tungsten oxide species was present on the alumina surface. On the other hand, above monolayer coverage, an easy-to-reduce, bulk-like WO_3 species in the form of crystallites (3−10 nm in size) was present on the surface, which led to the observed decrease in the temperature requirement.[22] X-ray absorption near edge spectroscopy (XANES) and Raman spectroscopy data indicated that at low coverages (∼1/3 × ML) and dehydrated conditions, WO_3 surface species possessed a distorted tetrahedral molecular structure, while at higher coverages and hydrated conditions it exhibited octahedral symmetry.[21,30,31] Raman analysis of low coverage WO_3/Al_2O_3 also indicated distorted tetrahedral with W═O and W−O−W bonds present hinting at the possibility of both monomeric and dimeric units[31] similar to those observed on silica.[32] As the coverage increased to a near monolayer, XANES and Raman data suggested the presence of distorted octahedral WO_3 species.[31] These results have also been corroborated by UV-DRS measurements to provide the edge energies (E_g) and ligand to metal charge transfer (LCMT) band information. In particular, UV-DRS at low tungsten loadings (∼0.5 W/nm^2), ∼1/10 × ML, under hydrated and dehydrated conditions resulted in E_g values of 5.3 and 5.1 eV, respectively, and exhibited one LCMT at ∼228 nm, suggesting the presence of mono-tungstate WO_4 surface species. On the other hand, at circum-monolayer loading (∼4.5 W/nm^2), E_g values at hydrated and dehydrated conditions were 4.1 and 4.0 eV, respectively, and several LCMT bands were observed at ∼228 and 254 nm. It was concluded that a mixture of mono- and poly-tungstates existed on the surface as indicated by the intermediate E_g value and multiple LCMT bands.[5,21] It was proposed that the change in the nature of the surface species (i.e., mono- vs di- vs poly-tungstate) as the tungsten oxide loading increased was related to the strong Brønsted acid sites which were spectroscopically observed at coverages of 1.4 W/nm^2 (1/3 × ML) and above.[5] In situ Raman spectra revealed that addition of K_2O to the supported WO_3/Al_2O_3 catalyst increased the concentration of isolated surface WO_x species and did not form K_2WO_4 nanoparticles at near monolayer coverage.[19]

Although the Al_2O_3 surfaces and its polymorphs α- and the γ-have been studied theoretically by Raybaud et al.,[33−36] much less effort has been directed into computationally modeling the structure and properties of active WO_x sites on Al_2O_3 and interactions of WO_x with the support. McBriarty et al.[37] modeled adsorbed, octahedral, 6-coordinated WO_x on α-$Al_2O_3(0001)$ surface at 0.5 × ML and showed that the protonation of oxidized WO_x/α-$Al_2O_3(0001)$ is not stable—a result in agreement with the experimental observation of nonfacile reducibility at lower tungsten loadings.[22] Monomeric WO_x or dimeric −O−W−O−W−O− species were used with W−O(OH) and W−$(OH)_2$−termination bonded to O-terminated α-$Al_2O_3(0001)$.[38] These hydroxyl groups on WO_x moiety acted as Brønsted sites for NH_3 adsorption. However, the exact structure of WO_x supported on Al_2O_3 with and without K_2O at catalytically relevant temperatures and their structure−function relationships have not yet been characterized at the atomic level using ab initio methods despite abundantly available experimental data. It is already known that the WO_x−Al_2O_3 interactions considerably influence the electronic and geometric properties of the surface species and their stability and reactivity. Therefore, it is crucial to model such systems to improve our understanding them and to help design better ones in the future. In the present study, density functional theory (DFT) calculations are used to model structural and vibrational properties of the isolated monomeric WO_3/Al_2O_3 and $K_2O/WO_3/Al_2O_3$ sites. The results are compared with the in situ Raman spectra of the catalysts, while changes in acidity are computed using NH_3 as a probe molecule.

THEORETICAL AND EXPERIMENTAL DETAILS

Quantum Chemical Calculations. All calculations are performed using ab initio plane-wave pseudopotential approach as implemented in VASP.[39,40] The PW91 functional[41] has been chosen to perform the periodic DFT calculations. The valence electrons are treated explicitly and their interactions with the ionic cores are described by the projector augmented-wave method,[42] which allows to use a low energy cutoff equal to 400 eV for the plane-wave basis. The Gamma point is used in the Brillouin-zone integration. The positions of all the atoms in the super cell are relaxed, until the total energy differences decrease below 10^{-6} eV (forces acting on atoms fall below 0.005 eV/Å).

DOI: 10.1021/acs.jpcc.8b08214
J. Phys. Chem. C 2018, 122, 24190−24201

Vibrational spectra have been calculated for selected surface species within the harmonic approximation. Only the W center atom and its first and second neighbors (O−Al and OH groups) are considered in the Hessian matrix. This matrix is computed by the finite difference method followed by a diagonalization procedure. The eigenvalues of the resulting matrix lead to the frequency values. The assignment of the vibrational modes is done by inspection of the corresponding eigenvectors. The Raman intensities were estimated by the derivative of the macroscopic dielectric tensor (polarizability) with respect to the normal mode, following the method of Fonari and Stauffer.[43]

Surface Model Description. The surface slab model was adopted from the previous work.[36,44] In particular, 5-layer (110) surface termination of γ-Al_2O_3 model $Al_{24}O_{36}$ was utilized as shown in Figure 1 with two bottom layers frozen during the optimization. This is due to the higher reactivity of Al_2O_3(110) termination toward adsorbing mononuclear species, such as $HReO_4$.[45] Al_2O_3(110) surface also possesses low-coordinated Al^{III} and Al^{IV} sites, which present efficient acceptor orbitals of low energy and form via truncation of tetra-coordinated Al atoms that are specific to the γ-Al_2O_3 structure.[45,46] Al^{IV} are derived from aluminum atoms inherited from bulk octahedral aluminum atoms, and Al^{III} are derived from aluminum atoms originating from bulk tetrahedral aluminum atoms.[44] After surface relaxation, Al^{IV} obtain pseudotetrahedral coordination, whereas Al^{III}—pseudoplanar. The topmost surface oxygen atoms are of μ_2−O and μ_3−O coordination. The unit cells have a dimension of 8.068 × 8.397 Å^2, corresponding to a W coverage of 1.47 nm^{-2}, which is approximately 1/3 ML.

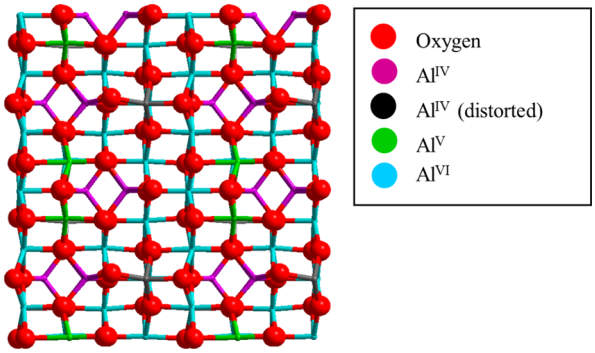

Figure 1. γ-Al_2O_3(110) surface showing the different coordinations of Al. It should be noted that sites exposed at the surface have one coordination number less.

Relative stability of the species was evaluated at 550 K using Boltzmann population via 1

$$p\ (\%) = \frac{e^{(-\Delta\Delta E_{ads}/kT)}}{\sum e^{(-\Delta\Delta E_{ads}/kT)}} \quad (1)$$

where k = 8.617 × 10^{-5} eV/K, ΔE_{ads} is 0 K adsorption energy without any vibrational corrections, and T = 550 K.

Synthesis of Model-Supported WO_3/Al_2O_3 and $K_2O/WO_3/Al_2O_3$ and in Situ Raman Analysis of Their Surface Structure. WO_3/Al_2O_3 and $K_2O/WO_3/Al_2O_3$ catalysts were prepared by co-impregnation of KOH and ammonium metatungstate [$(NH_4)_6H_2W_{12}O_{40}{\cdot}xH_2O$, 99.9%+ purity] on γ-Al_2O_3(surface area ≈ 170 m^2/g), drying under ambient conditions for 8 h, 120 °C for 16 h and subsequent calcination at 500 °C for 4 h. Raman spectra of dehydrated samples were taken with a visible (532 nm) laser excitation on a single-stage HORIBA-Jobin Yvon Lab Ram-HR Raman spectrometer equipped with a confocal microscope (Olympus BX-30) and a notch filter (Kaiser Super Notch). The visible excitation was generated by an Nd-YAG doubled diode pumped laser (Coherent Compass 315M-150; output power, 150 mW; sample power, 10 mW) with the scattered photons directed into a single monochromator and focused onto a UV-sensitive liquid-N_2 cooled CCD detector (HORIBA-Jobin Yvon CCD-3000V) with a spectral resolution of ∼2 cm^{-1} for the given parameters.

RESULTS AND DISCUSSION

Molecular Structure of WO_3 Species on γ-Al_2O_3(110). First, a systematic study on the possible configurations of the surface species resulting from H_2WO_4 grafting was investigated using computational methods. As shown in Figure 2, the H

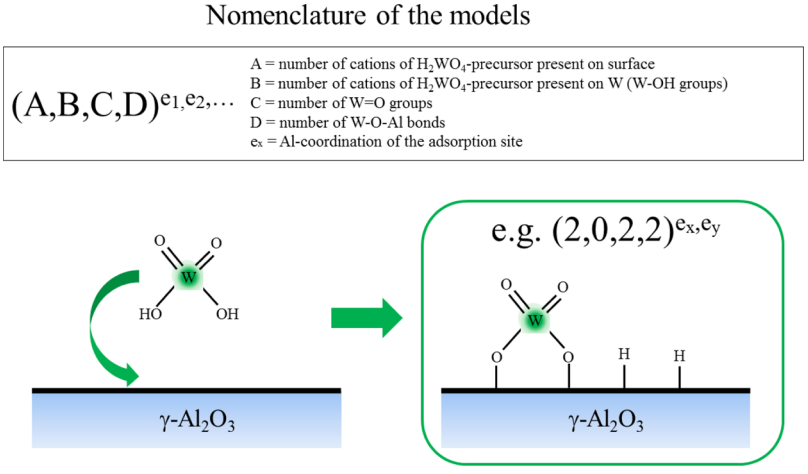

Figure 2. Conceptual surface site model nomenclature shown using a schematic representation of the grafting modes of the W precursor H_2WO_4. Surface K_2WO_4 isolated model site is obtained by substituting two protons with K^+ atoms to maintain charge neutrality. The superscript e indicates the oxygen to which it is coordinated and can be have up to six different e_x, e_y, ... values, according to the coordination sphere of tungsten observed in the model.

DOI: 10.1021/acs.jpcc.8b08214
J. Phys. Chem. C 2018, 122, 24190−24201

atoms can be placed around the W center or on surface oxygen forming a surface hydroxyl group.

Eighteen different configurations of these WO_x species were studied computational on different grafting sites on the γ-$Al_2O_3(110)$ surface. The relative total energies, shown in Table 1, indicate a competition (ΔE = 0.17 eV) between the

Table 1. Adsorption Energy, Relative Adsorption Energy, and Boltzmann Population at 550 K for the 18 Grafting Configurations (H_2WO_4) Studied[a]

configuration	ΔE_{ads}	$\Delta\Delta E_{ads}$	Boltzmann population p, %
$(1,1,1,3)^{4,5,5,6,6}$	−4.43	0.00	97
$(2,0,1,4)^{4,4,5,5,6}$	−4.25	0.17	3
$(1,1,1,2)^{4,4}$	−4.12	0.30	
$(1,1,0,4)^{4,5,5,6}$	−4.04	0.38	
$(2,0,2,3)^{4,4,5}$	−4.02	0.41	
$(2,0,2,3)^{4,5,5}$	−3.86	0.57	
$(2,0,2,2)^{4,4}$	−3.84	0.58	
$(1,1,0,4)^{4,4,5,5,6}$	−3.39	1.04	
$(0,2,0,4)^{4,4,4,5}$	−3.16	1.27	
$(2,0,1,3)^{4,5,5}$	−2.82	1.61	
$(0,2,0,4)^{4,4,4,5,5,5}$	−2.52	1.90	
$(1,1,1,3)^{3,5,5}$	−1.66	2.77	
$(1,1,1,2)^{5,5}$	−1.58	2.85	
$(0,2,0,3)^{3,5,5}$	−1.21	3.22	

[a]Energies in eV.

structure $(1,1,1,3)^{4,5,5,6,6}$ and $(2,0,1,4)^{4,4,5,5,6}$, that is, a WO_x with one oxo and one hydroxyl group and a W monomer with one oxo group. These are shown in Figure 3. The most stable

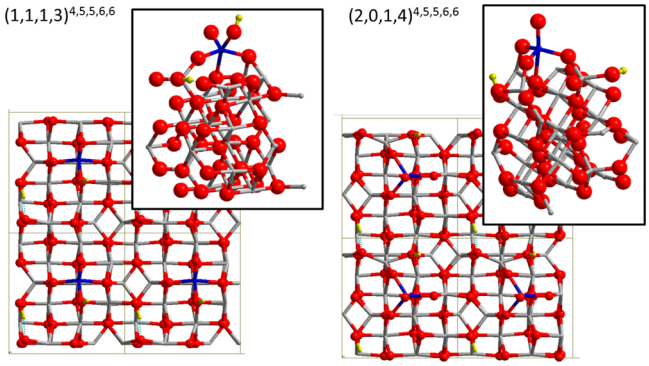

Figure 3. Two most stable configurations of WO_x species resulting from H_2WO_4 grafting on the γ-$Al_2O_3(110)$ surface. (Color code: blue: W, red: O, gray: Al, and yellow: H).

structure with an undissociated W precursor $(0,2,4)^{4,4,4,5}$ is 1.27 eV higher in energy compared with the most stable structure $(1,1,1,3)^{4,5,5,6,6}$. It is clear that the monomer species with two hydroxyl groups on the W center are energetically unfavorable (by more than 1 eV), and can thus be eliminated from the list of possible stable W oxide monomer species on the surface. The species with only one W═O or one W−OH group are at least 0.4 eV higher in energy, compared with the $(1,1,1,3)^{4,5,5,6,6}$ structure, which can also be considered energetically unfavorable (or, from another perspective, energetically activated). In general, grafted species were stabilized when the present W−OH groups are oriented toward the surface, in order to form H-bonds with the surface. The WO_x species were also more stabilized when its coordination is maximized up to 6, surrounded preferably by Al atoms in coordination: 6, 4, 5, and 3. Species having protons on γ-$Al_2O_3(110)$ bound to 3-coordinated oxygen atoms were also stabilized.

In the $(1,1,1,3)^{4,5,5,6,6}$ structure, the W═O and the W−OH bond lengths are 1.71 and 1.89 Å, respectively. The W−OAl bond lengths are 1.97, 1.84, and 2.17 Å. In the $(2,0,1,4)^{4,4,5,5,6}$ structure, the W═O bond distance is 1.72 Å. The W−OAl bonds are 1.85, 1.86, 1.90, and 2.30 Å. For comparison, the tungstenyl W═O bonds have lengths between 1.71 and 1.74 Å on amorphous silica,[32] which are comparable to our results.

Effect of K^+ Promotion on the Surface WO_x/γ-$Al_2O_3(110)$ Molecular Structure. Alkali metal ion doping is known to modify the acid−base character of tungsten oxide catalysts.[13,15,19,20] For example, addition of 5.0% K_2O wt to 19% WO_3/Al_2O_3 increased the population of the isolated surface WO_x species.[19] The shift of the W═O Raman band from 1021 to 963−985 cm^{-1} indicated that potassium atom was interacting with the surface WO_x species and elongating the W═O bond.[30] In the absence of K^+, the isolated surface WO_x sites on Al_2O_3 were difficult to reduce. However, addition of K_2O made the surface WO_x sites more reducible at elevated (>650 °C) temperatures.[19] Strong acidic gas molecules, such as SO_2, were found to preferentially bind to K_2O because of the strong K_2O basicity and its interaction with surface WO_x. To investigate the effects of K^+ promotion, the models were constructed starting from the H_2WO_4 structures, discussed in the previous section, placing the K^+ cations next to the W monomer. To preserve charge neutrality, WO_x and surface bound protons were substituted with K atoms. The substitutions of H^+ by K^+ yielded less complex model diversity, that is, different models converged to the same final optimized geometry. The grafting site, that is, the coordination of the W−O−Al Al atoms, was altered in some cases by the effect of relaxation because of the electrostatic forces introduced by the K^+ cations, which leads to less geometrically different models. A new nomenclature was adopted consisting of only two numbers and the coordination of the Al atoms on which the W monomer is grafted. The two numbers were the number of W═O bonds and the number of W−O−Al, linkages. The resulting adsorption energies together with the relative energy and the computed Boltzmann populations are shown in Table 2.

The two most stable geometries (see Table 2) for K_2WO_4 grafting on the γ-$Al_2O_3(110)$ surface were obtained from the following initial structures $(2,0,2,2)^{4,4}$ and $(1,1,1,3)^{3,5,5}$ for the first structure $(2,2)^{4,4}$ and from structure $(1,1,1,2)^{4,4}$ for the second structure $(2,2)^{4,5}$. Both structures are iso-energetic, showing only a difference in the position of the cations and the position of the WO_4 species on the surface. In the first structure, the cation is positioned closer to the W═O group than in the second one (see Figure 4). In structure $(2,2)^{4,4}$, the intercation distance is 4.50 Å and the W═O bond length is 1.75−1.79 Å. The closest distance between K^+ and W═O oxygen is 3.03 Å. In structure $(2,2)^{4,5}$, the intercation distance is 4.33 Å and the W═O bond length is 1.77−1.78 Å. The closest distance between K^+ and W═O oxygen is 2.72 Å. Starting from the different conformations and the corresponding proton positions shown in Table 2, an interesting observation emerges. One can clearly see that the potassium cations prefer to interact with the surface rather than with the WO_x monomer. Via the newly formed O−K bond, these K^+ cations interact directly with the γ-$Al_2O_3(110)$ surface, for

DOI: 10.1021/acs.jpcc.8b08214
J. Phys. Chem. C 2018, 122, 24190−24201

Table 2. Adsorption Energy, Relative Adsorption Energy, and Boltzmann Population at 550 K for the K^+ Promoted WO_x/γ-$Al_2O_3(110)$ Grafting Configurations Studied[a]

configuration	starting configuration	ΔE_{ads}	$\Delta\Delta E_{ads}$	Boltzmann population p, %
$(2,2)^{4,4}$	$(2,0,2,2)^{4,4}$, $(1,1,1,3)^{3,5,5}$	−4.86	0.00	37
$(2,2)^{4,5}$	$(1,1,1,2)^{4,4}$	−4.85	0.004	34
$(2,2)^{4,4^2}$	$(2,0,2,3)^{4,4,5}$	−4.78	0.07	8
$(2,3)^{4,5}$	$(2,0,1,3)^{4,5,5}$, $(1,1,1,3)^{3,5,5}$	−4.77	0.09	6
$(1,4)^{4,4,4,5,6}$	$(1,1,0,4)^{4,5,5,6}$	−4.71	0.14	2
$(2,2)^{4,4,4}$	$(0,2,0,4)^{4,4,4,5,5,5}$	−4.68	0.18	1
$(2,2)^{4,4,5}$	$(2,0,2,3)^{4,5,5}$, $(1,1,0,4)^{4,4,5,5,6}$	−4.61	0.25	
$(1,4)^{4,4,4,4,4}$	$(2,0,1,4)^{4,4,5,5,6}$	−4.57	0.29	
$(2,2)^{4,4,5}$	$(1,1,1,3)^{4,5,5,6,6}$	−4.36	0.49	
$(2,2)^{4,5}$	$(1,1,1,2)^{5,5}$	−3.10	1.76	
$(2,2)^{4,4}$	$(0,2,0,3)^{3,5,5}$	−2.04	2.82	

[a]Energies shown are in eV.

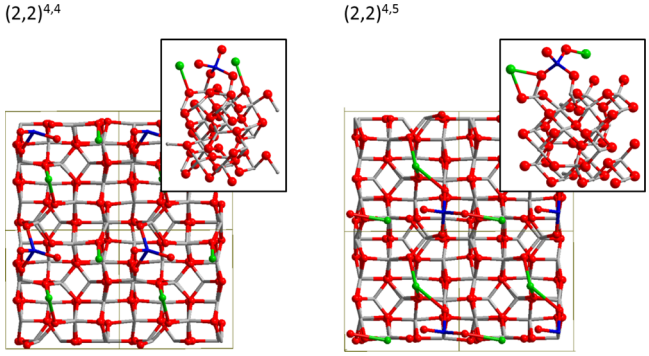

Figure 4. Two most stable configurations for K_2WO_4 grafting on the γ-$Al_2O_3(110)$ surface. (Color code: blue: W, red: O, gray: Al, and green: K).

example, the W−O−Al bridge site is not particularly preferred compared with the Al−O−Al bridge for the interaction with K^+. The O−W−O site bonded to K^+ destabilizes the system (see Table 2, the least stable $(2,2)^{4,4}$ structure). Another interesting observation to notice is that the K^+ cations are separated by about 4.5 Å within the unit cell due to the coverage. The grafting site is dominated by distorted Al atoms with coordination number of 4 and, to a lesser extent, coordination number of 5. It follows that with increasing W coverage, the equivalent K^+ doping will tend to destabilize the catalyst, for example, increase the relative energy of the overall system. It is interesting to note that the most stable H_2WO_4 system $(1,1,1,3)^{4,5,5,6,6}$ is destabilized after the substitution of H^+ with K^+ because of a strong distortion of the tetrahedral configuration of WO_x and electrostatic destabilization of the W−O−Al linkages. In the contrary, one of the most unstable (i.e., the most reactive H_2WO_4) systems—$(1,1,1,3)^{3,5,5}$—is strongly stabilized after substitution of H^+ by K^+. Indeed, the W tetrahedral configuration is respected and K^+ is stabilized by the surface oxygen atoms. The position of the cation at this coverage is clearly determined by the strong electrostatic interactions. The most energetically optimal position should have a maximum coordination of the cation. The types of oxygen atoms that were used as coordination sphere is important, for example, W═O oxygen atoms, Al−O−W oxygen atoms, and Al−O−Al oxygen atoms. Moreover, there can be, in the proximity of the acidic center, a competition with the redox centers (W atoms). Combining this with the molecular structure and coordination to the surface of WO_x, three coordination groups can be distinguished, based on their relative stability: (a) the structures containing mono-oxo W species, (b) di-oxo species with a minimal distorted tetrahedral configuration with K^+ cations positioned near high coordination sites, and (c) di-oxo species with tetrahedral configuration destabilized by under-coordinated K^+ cations present close to the W═O oxygen atom.

Raman Spectroscopy and Theoretical Spectra Calculations of WO_x/Al_2O_3 and $K_2O/WO_x/Al_2O_3$. Experimental Raman spectra of 5% WO_x/Al_2O_3 and 2.5% K_2O/5% WO_x/Al_2O_3 sites with concentrations expressed in weight percent of metal are shown in Figure 5. Raman spectra of the crystalline

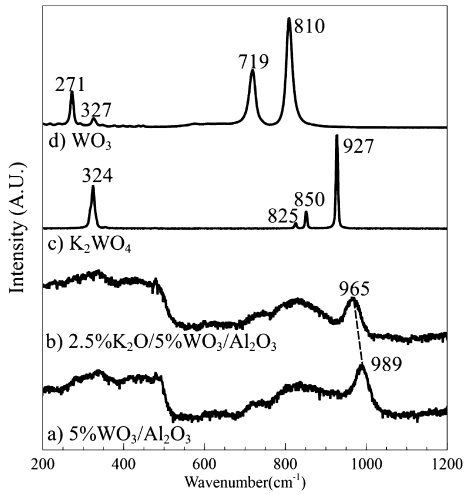

Figure 5. Raman spectrum for (a) 5% WO_x/Al_2O_3, (b) 2.5%K_2O/5% WO_x/Al_2O_3, (c) K_2WO_4, and (d) WO_3.

WO_3 and K_2WO_4 reference compounds are shown for reference. Crystalline WO_3 exhibits strong Raman bands at 271, 719, and 810 cm^{-1}, whereas crystalline K_2WO_4 possesses intense Raman bands at 324 and 927 cm^{-1}. The spectra are consistent with the oligomeric WO_6 and isolated WO_4 sites present in the bulk WO_3 and K_2WO_4 crystals, respectively.[19,21] The Raman spectra of the dehydrated supported 5% WO_x/Al_2O_3 and 2.5% K_2O/5% WO_x/Al_2O_3 catalysts are also shown in Figure 5. The Raman spectrum of supported 5% WO_3/Al_2O_3 exhibits a band at 989 cm^{-1}, and the absence of characteristic Raman bands from crystalline WO_3 indicates that the supported tungsten oxide phase is only present as surface WO_x species on the Al_2O_3 support. This Raman band at 989 cm^{-1} corresponds to the stretching mode of isolated and oligomeric mono-oxo $O{=}WO_{4/5}$ surface species.[47] The Raman spectrum for the K^+-promoted supported 2.5%K_2O/5%WO_x/Al_2O_3 catalyst exhibits the W═O band at 965 cm^{-1}. The absence of strong and sharp Raman bands from crystalline K_2WO_4 reveals that the supported tungsten oxide phases are present as surface WO_x species on the alumina support.[48] The shift of the W═O Raman band from 989 to 965 cm^{-1} indicates that the potassium is interacting with the surface WO_x species and results in lengthening of the W═O bond.[48] These data are also consistent with the literature observations, where the addition of K_2O for the supported near monolayer coverage 19% WO_x/Al_2O_3 catalyst increased the UV−vis E_g

DOI: 10.1021/acs.jpcc.8b08214
J. Phys. Chem. C 2018, 122, 24190−24201

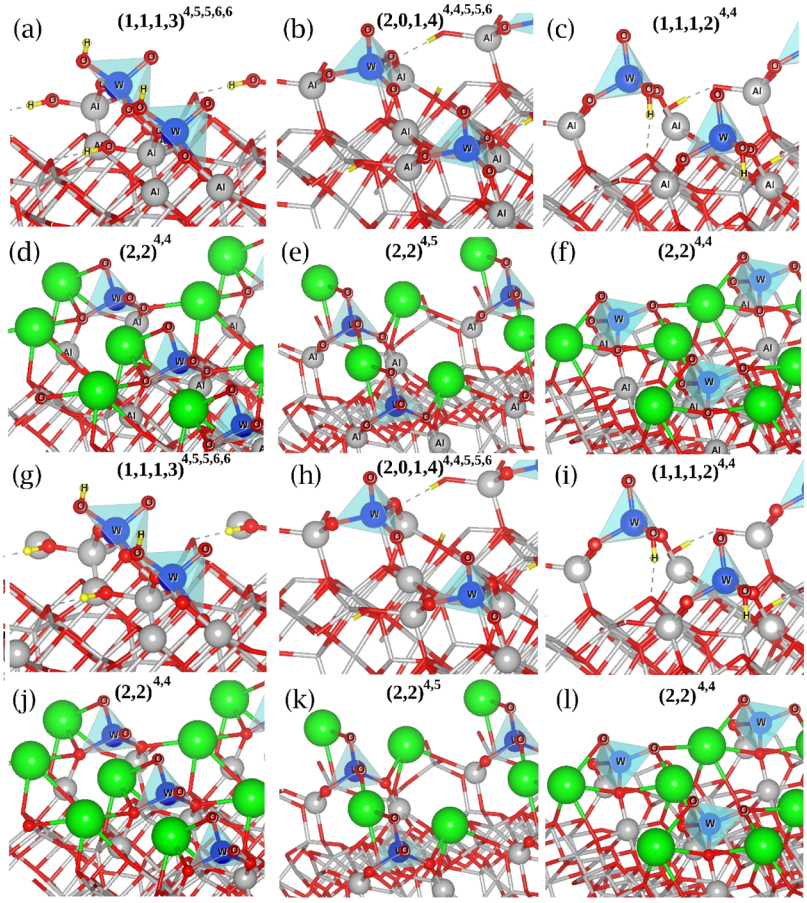

Figure 6. Molecular structures used to obtain the theoretical Raman spectra, where only the atoms labeled with letters were relaxed during the geometry optimization. (gray: Al, blue: W, red: O, yellow: H, green: K). Resulting spectra are shown in Figure 7.

value to 4.9 eV showing an increase in the population of isolated surface WO_x species at the expense of the oligomeric surface WO_x species.[19]

Next, we computed Raman bands of the three lowest energy structures $(1,1,1,3)^{4,5,5,6,6}$, $(2,0,1,4)^{4,4,5,5,6}$, and $(1,1,1,2)^{4,4}$ of WO_x/γ-$Al_2O_3(110)$ structures shown in Table 1 and $(2,2)^{4,4}$, $(2,2)^{4,4}$, and $(2,2)^{4,4}$ K^+-promoted WO_x/γ-$Al_2O_3(110)$ structures shown in Table 2 (here, the two $(2,2)^{4,4}$ structures ($(2,2)^{4,4}$ and $(2,2)^{4,4'}$) originated from the three different original protonated structures, namely $(2,0,2,2)^{4,4}$, $(1,1,1,3)^{3,5,5}$, and $(2,0,2,3)^{4,4,5}$) that are similar but not identical. The structures used to obtain the theoretical Raman spectra are shown in Figure 6. In particular, Figure 6a–f identifies structures with WO_x moiety and the nearest neighbors relaxed during the frequency calculations for WO_x/γ-Al_2O_3 and K^+-promoted WO_x/γ-Al_2O_3, respectively. Figure 6g through l shows the molecular structure with only the corresponding O═W═O(H) moiety relaxed.

All Raman spectra were normalized to the peak of the highest intensity here corresponding to that of W═O═W symmetric stretch at around 980 cm^{-1}. The resulting spectra are shown in Figure 7. In particular, the dashed line spectra correspond to the calculations where a W atom center and its first and second neighbors (O, OH, and O–Al groups) were relaxed (see Figure 6a–f). The shaded spectra correspond to the Raman vibrations where only the W atom center and the atoms not linked to the surface (O and OH) were allowed to relax (see Figure 6g–l). This procedure was developed to decouple majority Al–O–W contribution, which otherwise could result in a broad and complex peak structure.

The unpromoted WO_x/γ-Al_2O_3 catalyst exhibits a characteristic measured Raman band at 989 cm^{-1} (see Figure 5) corresponding to the W═O vibration. Experimentally, however, other vibrational contributions are rarely reported and derived computational models present a unique opportunity to describe the overall Raman vibrational system. Structure $(1,1,1,3)^{4,5,5,6,6}$ shows, besides the typical WO–H stretching mode at 3857 cm^{-1}, a W═O stretching at 984 cm^{-1}. This too good agreement is probably due to canceling of errors often encountered in DFT calculations.[49] The W–OH stretching is found at 709 cm^{-1}, which could correspond the experimental broad and difficult to resolve 721 cm^{-1} band. An antisymmetric OH stretch is observed at 600 cm^{-1}. Finally, the low frequency modes observed in theoretical Raman spectrum are difficult to distinguish in the experimental one. For structure $(2,0,1,4)^{4,4,5,5,6}$, the experimental W═O vibration frequency is also predicted correctly, which corresponds to a tri-coordinated W═O stretching mode at 979 cm^{-1} in the calculated Raman spectrum. This is only 5 cm^{-1} lower compared with the bi-coordinated $(1,1,1,3)^{4,5,5,6,6}$ (HO)W═O stretching. Other low frequency bands are shown in Table 3, and because of the complexity of the experimental spectra, the matching is difficult to observe. This interesting observation has implications for the experimental spectra. Often discussed and assigned mono-oxo WO_x species ascribed to the peak at ~980 cm^{-1} can also be due to the partially hydrated (HO)W═O moiety-containing species. If the proton is not

DOI: 10.1021/acs.jpcc.8b08214
J. Phys. Chem. C 2018, 122, 24190–24201

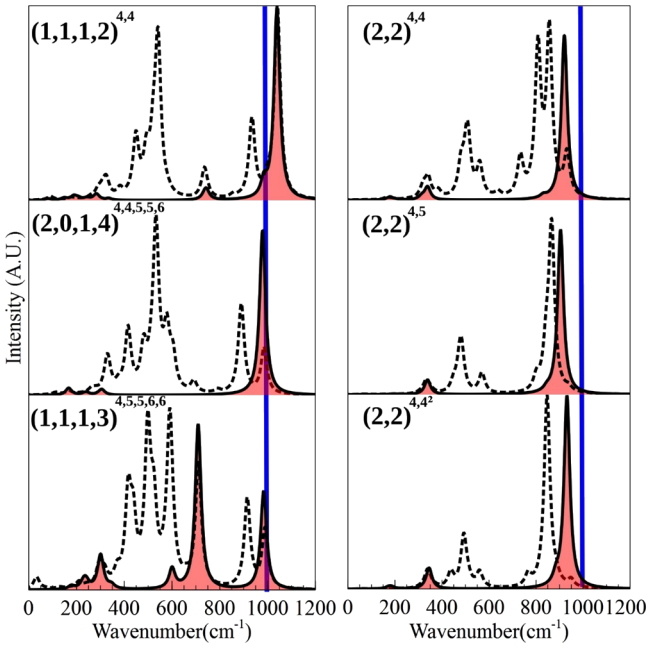

Figure 7. Calculated Raman spectra of WO_x/γ-Al_2O_3(left side) and K^+-promoted WO_x/γ-Al_2O_3(right side) structures shown in Figure 6 obtained between 1200 and 0 cm^{-1}. Dashed line spectra: a W center and its first and second neighbors (O and OH) are relaxed. Color spectra: only atoms not linked to the surface (W, O, and OH) are relaxed. Blue vertical line corresponds to 980 cm^{-1} value obtained in Raman experiments of isolated WO_x species.

H-bonded to any neighboring atom, its bending vibration will not be present at 1039 cm^{-1} as in $(1,1,1,2)^{4,4}$ case (vide infra) and the distinction between pure di-oxo and mono-oxo hydroxylated moieties will not be possible experimentally but not theoretically. The only distinction, as shown in Figure 7, between di-oxo and mono-oxo hydroxylated WO_x can be a strong $\nu_a(W{=}O_hH)$ vibration at 600 cm^{-1} in the $(1,1,1,3)^{4,5,5,6,6}$ structure, not present in $(2,0,1,4)^{4,4,5,5,6}$. Finally, in the $(1,1,1,2)^{4,4}$ structure containing a WO−H group hydrogen-bonded to the surface, a OH stretching mode at 3074 cm^{-1} is present with the corresponding strong bending mode calculated at 1039 cm^{-1}. The W═O has a stretching mode at 985 cm^{-1}. Stretching W−OH vibrations are observed at 743 cm^{-1}. The low frequency bands assignments are attributed to other stretching, bending, and libration modes. Notably, the Raman band at 1015 cm^{-1} has previously been assigned to surface WO_5/WO_6 poly-tungstate like species after dehydration at 450 °C but not on the samples exposed to ambient conditions.[21] Our data thus suggest that an alternative assignment to this peak as the shift toward higher wavenumbers, typically associated with bond elongation, can potentially also occur due to the (O)═W−OH moiety.

An analysis of the Raman spectra, which include first and second neighbors of W (dashed line in Figure 7), allowed us to conclude that the peaks between 890 and 920 cm^{-1} might be attributed to W═O−Al stretching modes. The peaks in the range from 330 to 560 cm^{-1} include O−Al−O superficial and W═O−Al vibrational modes. Hence, when comparing the calculated total DFT spectra with the corresponding experimental, the relative intensities of the vibrations involving WO_x and those involving O−Al−O superficial and W═O−Al (effectively the support) support need to be taken into account. The O−Al−O superficial and W═O−Al vibrations

Table 3. Calculated Raman Wavenumbers of Atoms Not Linked to the Surface (O and OH) Corresponding to the Different Types of Vibrations: a-Antisymmetric, s-Symmetric, ν-Stretching, δ-Bending, and L-Libration (R-Rocking, W-Wagging, and T-Twisting)[a]

freq	assign.	freq	assign.	freq	assign.	freq	assign.	freq	assign.
H_2WO_4 precursor						K_2WO_4 precursor			
$(1,1,1,3)^{4,5,5,6,6}$		$(2,0,1,4)^{4,4,5,5,6}$		$(1,1,1,2)^{4,4}$		$(2,2)^{4,4}$		$(2,2)^{4,5}$	
				1039	$\delta(W{=}O_hH)$				
984	$\nu(W{=}O)$	979	$\nu(W{=}O_s)$	985	$\nu(W{=}O_s)$	931	$\nu_s(O{=}W{=}O)$	904	$\nu_s(O{=}W{=}O)$
						884	$\nu_a(O{=}W{=}O)$	848	$\nu_a(O{=}W{=}O)$
709	$\nu(W{=}O_h)$			743	$\nu(W{=}O_H)$	345	$\delta(O{=}W{=}O)$	334	$W(O{=}W{=}O)$
600	$\nu_a(W{=}O_hH)$								
346	$W(O{=}W{=}O_h)$								
300	$W(O{=}W{=}O_h)$	306	$\nu(W{=}O) + \delta(O{=}W{=}O_s)$	283	$\delta(O_h{=}W{=}O_s)$				
224	$\delta(O{=}W{=}O_h) + W(W{=}O_hH)$			207	$\delta(O_h{=}W{=}O_s) + \nu_s(O{=}W{=}O)$				
179	$W(W{=}O_hH)$	170	$W(O{=}W{=}O)$	189	$\nu_a(O{=}W{=}O) + \delta(O_h{=}W{=}O)$	183	$R(O{=}W{=}O)$		

freq	assign.	freq	assign.
		$(2,2)^{4,4^2}$	
920	$\nu_s(O{=}W{=}O)$		
830	$\nu_a(O{=}W{=}O)$		
338	$\delta(O{=}W{=}O)$		
316	$W(O{=}W{=}O)$		
180	$R(O{=}W{=}O)$		

[a] O_h—oxygen atom bonded with hydrogen.

DOI: 10.1021/acs.jpcc.8b08214
J. Phys. Chem. C 2018, 122, 24190−24201

should be weighed over different representative models. This will result in an increased WO_x vibration and explain why experimental Raman spectra of WO_x/Al_2O_3 in this work and in the references lack any discernible peaks below 900 cm^{-1}.

The presence of K^+ results in the W═O symmetric stretching red-shift to 965 cm^{-1} experimentally, as shown in Figure 5. Our calculations predicted a stronger shift to ~920 cm^{-1} in all three lowest energy structures, namely $(2,2)^{4,4}$, $(2,2)^{4,5}$, and $(2,2)^{4,4^2}$. In $(2,2)^{4,4}$, symmetric stretching is found at 931 cm^{-1}, antisymmetric stretching at 884 cm^{-1}, and bending O═W═O mode at 345 cm^{-1}. Other libration modes are observed on low frequency ranges. For both $(2,2)^{4,5}$ and $(2,2)^{4,4^2}$ structures, the W═O stretching is calculated at 904 and 920 cm^{-1}, respectively. It is interesting to note that these are nearly equal to the one observed in K_2WO_4 in Figure 5. In a similar way as with the unpromoted WO_x spectral calculations, 890−920 cm^{-1} region peaks are attributed to W═O−Al stretching modes while those between 330 and 560 cm^{-1} to other O−Al−O superficial and W═O−Al vibrational modes. These data are apparent from Figure 7 dashed line simulated spectra. We propose that experimental spectra will have very complex (and hence broadened) contributions from the surface bonds, difficult to resolve. Hence, a single peak is mostly pronounced for these species, WO_x and K^+ promoted WO_x alike. In the latter case, K^+ should result in even stronger bond polarizing effect.

In summary, the unpromoted and K^+ promoted structures, that reproduce the best experimental data, were $(1,1,1,3)^{4,5,5,6,6}$ and $(2,2)^{4,5}$, respectively. The other structures are also present on the surface but with lower populations. In other words, isolated WO_x species is expected to possess both ═O and OH groups on Al_2O_3 surface and K^+ promotion would result in a clear spectral shift regardless the final coordination of K^+ ions.

Surface Acidity Testing via DFT Calculations of NH_3 Adsorption on WO_3/Al_2O_3 and $K_2O/WO_3/Al_2O_3$. NH_3 is a probe molecule used in experimental acidity tests of the catalyst structures. Three cases of NH_3 were considered and calculated in this work, for example, on γ-Al_2O_3(110), WO_x/γ-Al_2O_3(110), and $K_2O/WO_x/\gamma$-Al_2O_3(110). The latter two correspond to the lowest energy, for example, $(1,1,1,3)^{4,5,5,6,6}$ and $(2,2)^{4,4}$ structures, in Tables 1 and 2. Several unique adsorption sites are present, as shown in Figure 8, that were explored on each surface and calculated the corresponding vibrational frequencies. Here, γ-Al_2O_3(110) is considered as fully dehydroxylated surface with primarily Lewis acid sites available.

The tabulated experimental vibrational frequencies of NH_3 adsorbed on γ-Al_2O_3, WO_3/γ-Al_2O_3, and $K_2O/WO_3/\gamma$-Al_2O_3 are shown in Table 4.

For γ-Al_2O_3, NH_3 adsorption yielded major bands at 3400, 3355, 1600, 1285, and 1230 cm^{-1}.[50,52] All of these bands were attributed to NH_3 coordinated to Lewis acid sites, given that the γ-Al_2O_3 was pretreated at temperatures higher than 400 °C and that almost no band corresponding to NH_3 adsorbed on Brønsted acid sites was observed for such samples.[50,52] On the other hand, when γ-Al_2O_3 was pretreated at temperatures less than 400 °C, extra bands were observed, which were attributed to NH_4^+ species on Brønsted acid sites. Major bands corresponding to NH_4^+ species on Brønsted acid sites are 3100, 1560, 1510, 1470, 1450, and 1410 cm^{-1}.[51] Therefore, the pretreatment temperature changes the nature of the acid sites present on the surface of γ-Al_2O_3, which also corresponds

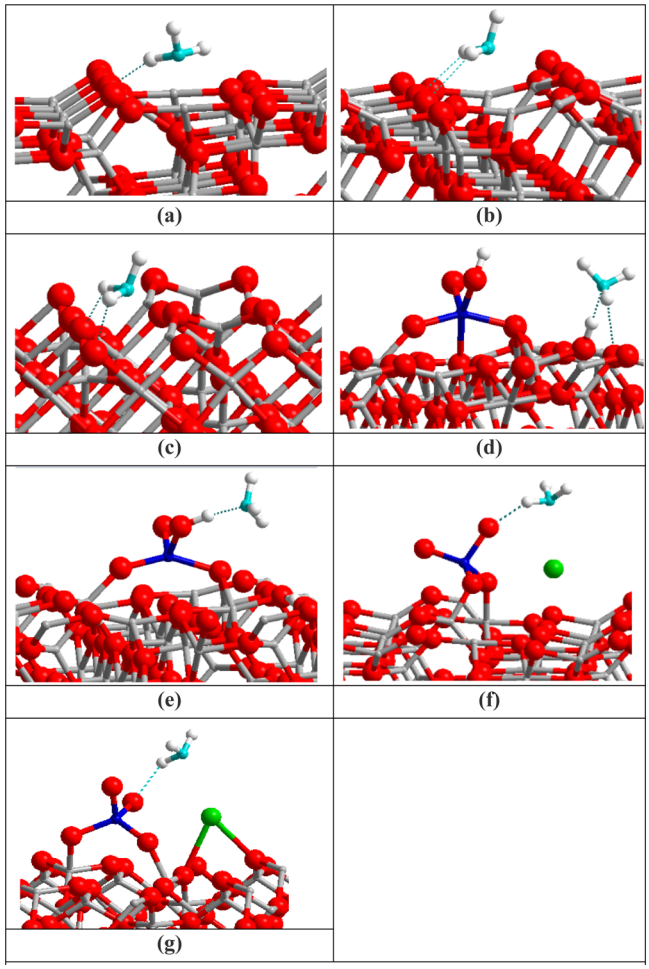

Figure 8. Computed NH_3 adsorbed structures on (a−c) γ-Al_2O_3(110), (d,e) WO_x/γ-Al_2O_3(110), and (f,g) $K_2O/WO_x/\gamma$-Al_2O_3(110).

to a change in the heat of adsorption of NH_3.[51] A comparison of calculated NH_3 adsorption bands on γ-Al_2O_3 shown in Figure 8a−c versus the observed experimental bands is shown in Figure 9. It can be seen that the experimental values agree well with the calculated values for all vibrational modes. Furthermore, the DFT calculations show a doublet at 1638 and 1586 cm^{-1} for NH_3 coordinated to two different Lewis acid sites or Lewis and Brønsted sites. However, experimental results only show a singlet at 1600−1610 cm^{-1} for Lewis acid sites. For pretreatment temperatures of <400 °C, the only other band in this region would be from NH_4^+ species on a Brønsted acid site at 1560 cm^{-1}.[51] However, the N−H stretch with a DFT calculated average value of 3184 cm^{-1} was not observed in experiments at all.

For 20% WO_x/Al_2O_3, NH_3 adsorption yielded major bands at 1674, 1615, 1432, and 1279 cm^{-1}.[19] The bands at 1615 and 1279 cm^{-1} were attributed to NH_3 coordinated to Lewis acid sites and the ones at 1674 and 1432 cm^{-1} were attributed to NH_4^+ on Brønsted acid sites.[19] In that study, the sample was pretreated at 400 °C, which is why both Lewis and Brønsted acid sites were observed. A comparison of DFT calculated NH_3 adsorption shown in Figure 8d,e versus the observed experimental bands is shown in Figure 9. The experimental values agree well with the calculated values for lower wavenumber modes (1200−1700 cm^{-1}), which correspond

DOI: 10.1021/acs.jpcc.8b08214
J. Phys. Chem. C 2018, 122, 24190−24201

Table 4. Summary of the Experimental Data for NH_3 Adsorption on γ-Al_2O_3, WO_3/γ-Al_2O_3, and $K_2O/WO_3/\gamma$-Al_2O_3

refs	details/comments	bands (cm^{-1})	description
50	NH_3 adsorption on γ-Al_2O_3	3400	coordinatively held NH_3 on Lewis acid sites
	adsorption conducted at 50 °C	3355	coordinatively held NH_3 on Lewis acid sites
	γ-alumina pretreated at 800 °C	3386	$-NH_2$
		3335	$-NH_2$
		3100	NH_4^+ on Brønsted acid sites
		1600	coordinatively held NH_3 on Lewis acid sites
		1510	$-NH_2$
51	NH_3 adsorption on γ-Al_2O_3	1230	coordinatively held NH_3 on Lewis acid sites
	adsorption conducted at 25 & 150 °C	1450, 1470	NH_4^+ on Brønsted acid sites
	γ-alumina pretreated at 330 °C	1600	NH_4^+ on Brønsted acid sites
		1560	coordinatively held NH_3 on Lewis acid sites (at 150 °C: NH_4^+ on Brønsted site or NH_2^-)
52	NH_3 adsorption on γ-Al_2O_3	1230, 1285	coordinatively held NH_3 on Lewis acid sites
	adsorption conducted at 25 °C		
	γ-alumina pretreated at 600 °C		
	NOTE: for alumina pretreated at temperatures >400 °C, almost no Brønsted sites were present. Brønsted sites would correspond to the following bands	1410, 1510, 1560	NH_4^+ on Brønsted acid sites
53	NH_3 adsorption on crystalline WO_3	3393, 3318, 3167, 1601, 1270, and 1221	coordinatively held NH_3 on Lewis acid sites
	adsorption conducted at 25, 100, 200, 250, 300 °C		
	WO_3 pretreated at 700 °C	3253, 3203, 1467, and 1395	NH_4^+ on Brønsted acid sites
19	NH_3 adsorption on isolated site 20% WO_x/Al_2O_3	1615	coordinatively held NH_3 on Lewis acid sites
	adsorption conducted at 120, 200, 300, 400 °C	1279	NH_4^+ on Brønsted acid sites
	catalyst pretreated at 400 °C	1674	
		1432	
19	NH_3 adsorption on isolated site 5%K_2O/19%WO_3/Al_2O_3	1646	coordinatively held NH_3 on K^+ sites
	adsorption conducted at 120, 200, 300, 400 °C		
	catalyst pretreated at 400 °C		

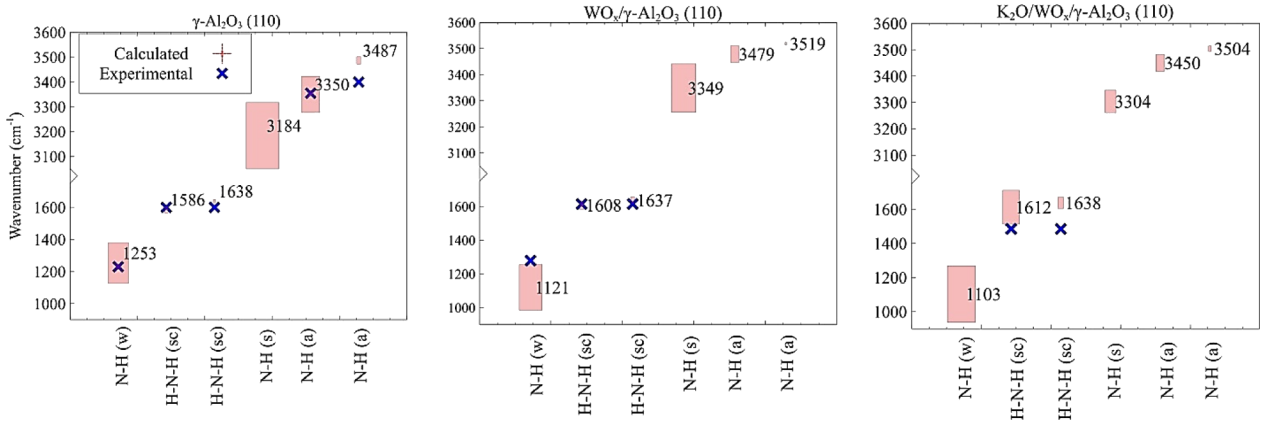

Figure 9. Comparison of the experimental (blue cross marks) and DFT calculated (shaded pink) values of adsorbed NH_3 vibrations on γ-Al_2O_3(110), WO_x/Al_2O_3(110), and $K_2O/WO_x/Al_2O_3$(110). Missing blue cross marks indicate that experimental data were not available for that vibration. The shaded pink region is the range of DFT calculated values for each vibration of NH_3 adsorbed on various sites. Tabulated frequencies of experimental NH_3 adsorption on γ-Al_2O_3, WO_x/Al_2O_3, and $K_2O/WO_x/Al_2O_3$ are summarized in Table 4.

to N−H wagging and H−N−H scissoring. However, the N−H stretches (symmetric & asymmetric) with calculated average values of 3349, 3479, and 3519 cm^{-1} were not found in experimental reports, according to the best of our knowledge.[19] The DFT calculations showed a doublet at 1637 and 1608 cm^{-1} for NH_3 coordinated to a W−OH moiety without resulting proton donation. However, experimental results only show a singlet at 1615 cm^{-1}. The only other band observed in the 1600−1700 cm^{-1} region came from NH_4^+ species on Brønsted acid site at 1674 cm^{-1}. Therefore, from our DFT calculated values, it cannot be ascertained if it is a vibration from NH_3 adsorbed on two different Lewis acid sites or if it is a

DOI: 10.1021/acs.jpcc.8b08214
J. Phys. Chem. C 2018, 122, 24190−24201

mixture of Lewis and Brønsted acid sites. Our calculations, however, show that NH_3 always prefers to bind to W−OH moiety via weak H-bonded interaction and peaks due to the Brønsted acid would likely result from the interaction with the Al_2O_3 support.

Lastly, NH_3 adsorption on 5% K_2O/19%WO_x/Al_2O_3 reported in the literature yielded a major band at 1646 cm^{-1}.[19] This band was attributed to NH_3 adsorbed onto a K site, and it was argued that addition of K effectively eliminated all acidity.[19] A comparison of calculated NH_3 adsorption bands versus the observed experimental bands is shown in Figure 9. The only experimental band observed was at 1646 cm^{-1}, and no other band was reported. The DFT calculations, however, showed calculated bands at 1103, 1612, 1638, 3304, 3450, and 3504 cm^{-1}. From Figure 8f,g it can be seen that NH_3 indeed binds to K^+ ions, thus confirming recent experimental assignments.[19] Our calculations also show that exact speciation of the adsorption site acidity with NH_3 in this complex system is rather challenging as all of the coordination modes result in a Lewis-like behavior.

Adsorption energies (ΔE_{ads}, eV) for various NH_3 adsorption sites shown in Figure 8 were calculated and are listed in Table 5. It can be clearly seen that γ-Al_2O_3(110) surface has the strongest adsorption (most exothermic ΔE_{ads} values), followed by WO_x/γ-Al_2O_3(110) and K_2O/WO_x/γ-Al_2O_3(110). The structures with K^+ have the weakest NH_3 adsorption (least exothermic values), as K^+ is a Lewis base so the basic NH_3 molecules have weakened (or very little) interaction with the surface. It is interesting to note that for WO_x/γ-Al_2O_3(110), the ΔE_{ads} values vary significantly from −0.71 versus −0.10 eV, depending on if the NH_3 is bonded to a proton on O−Al (catalyst support) or a proton on the W−OH (WO_x surface species) respectively. As the γ-Al_2O_3(110) support has a greater density of stronger acid sites, the NH_3 adsorption is more exothermic. Hence, temperature-programmed methods should allow us to distinguish the three different types of surface sites available on K_2O/WO_x/γ-Al_2O_3(110).

Table 5. Calculated Adsorption Energy (ΔE_{ads}) Values for NH_3 Structures Shown in Figure 8: (a−c) γ-Al_2O_3(110), (d,e) WO_x/γ-Al_2O_3(110), and (f,g) K_2O/WO_x/γ-Al_2O_3(110)

composition	case	ΔE_{ads} (eV)
γ-Al_2O_3(110)	A	−1.98
	B	−1.22
	C	−1.47
WO_x/γ-Al_2O_3(110)	D	−0.71
	E	−0.10
K_2O/WO_x/γ-Al_2O_3(110)	F	−0.47
	G	−0.45

CONCLUSIONS

In this study, the structure and Raman spectra of unpromoted and K^+-promoted tungsten oxide catalyst monomeric sites supported on γ-Al_2O_3(110) (K_2O/WO_x/γ-Al_2O_3(110)) were investigated using periodic DFT calculations and supporting Raman experiments. One WO_3-grafted monomer on the γ-Al_2O (110) surface was identified to be dominated by the $(1,1,1,3)^{4,5,5,6,6}$ structure together with the $(2,0,1,4)^{4,4,5,5,6}$ structure, with a total energy difference of 0.17 eV between both structures. Both structures showed W═O and W−OH groups along with three Al−O−W linkages. The grafted WO_3 species were stabilized when the present W−OH groups are oriented toward the alumina surface leading to the formation of H-bonds. This is different from the literature reports where distorted mono-oxo species are typically postulated and attributed to the experimental Raman band in 970−1014 cm^{-1}. It was also found that W−OH moiety bound to the surface support oxygen atoms (but not uncoordinated) can possess bending modes in the vicinity of those typically attributed to W═O vibrations. In the case of the K^+—promoted WO_x species, the $(2,2)^{4,4}$ and $(2,2)^{4,5}$ structures were the most stable. The W═O bond elongated in the presence of K^+ in agreement with the experimental observations with the Raman band at 989 that shifting to 965 cm^{-1}. The calculated W═O and W−OH vibrations were well localized in the calculated spectra and little shifts are observed upon the change in the WO_x geometry. Importantly, WO_x species, as suggested by our calculations, are expected to possess both W═O and W−OH groups from both energetics and vibrational arguments. For the most stable model structures, the adsorption of NH_3 was simulated to probe the acidity of the catalyst. The vibrational frequencies obtained suggested that NH_3 binds via Lewis-like coordination, even with the protons of W−OH or Al−OH groups. Calculated binding energies decrease in strength with NH_3 adsorbed on γ-Al_2O_3(110) > WO_x/γ-Al_2O_3(110) > K_2O/WO_x/γ-Al_2O_3(110) with some diversity found between W−OH···HNH_2 and Al−OH···HNH_2 groups.

AUTHOR INFORMATION

Corresponding Authors

*E-mail: frederik.tielens@vub.be (F.T.).
*E-mail: job314@lehigh.edu (J.B.).

ORCID

Frederik Tielens: 0000-0002-6760-6176
Jonas Baltrusaitis: 0000-0001-5634-955X

Notes

The authors declare no competing financial interest.

ACKNOWLEDGMENTS

This work by J.B. and D.K. was supported as part of UNCAGE-ME, an Energy Frontier Research Center funded by the U.S. Department of Energy, Office of Science, Basic Energy Sciences under award no. DE-SC0012577. This work used the Extreme Science and Engineering Discovery Environment (XSEDE),[54] which is supported by National Science Foundation grant number ACI-1053575. G.B. and P.Q. thank CONICET and UNL for financial support. Prof. Israel Wachs is acknowledged for assistance with Raman measurements.

REFERENCES

(1) Ma, Z.; Zaera, F. Heterogeneous Catalysis by Metals. *Encyclopedia of Inorganic Chemistry*; John Wiley & Sons, Ltd, 2006.
(2) Soultanidis, N.; Zhou, W.; Psarras, A. C.; Gonzalez, A. J.; Iliopoulou, E. F.; Kiely, C. J.; Wachs, I. E.; Wong, M. S. Relatingn-Pentane Isomerization Activity to the Tungsten Surface Density of WOx/ZrO2. *J. Am. Chem. Soc.* **2010**, *132*, 13462−13471.
(3) Baertsch, C. D.; Komala, K. T.; Chua, Y.-H.; Iglesia, E. Genesis of Brønsted Acid Sites during Dehydration of 2-Butanol on Tungsten Oxide Catalysts. *J. Catal.* **2002**, *205*, 44−57.
(4) Santiesteban, J. G.; Vartuli, J. C.; Han, S.; Bastian, R. D.; Chang, C. D. Influence of the Preparative Method on the Activity of Highly

DOI: 10.1021/acs.jpcc.8b08214
J. Phys. Chem. C 2018, 122, 24190−24201

Acidic WOx/ZrO2and the Relative Acid Activity Compared with Zeolites. *J. Catal.* **1997**, *168*, 431−441.
(5) Chen, X.; Clet, G.; Thomas, K.; Houalla, M. Correlation between structure, acidity and catalytic performance of WOx/Al2O3 catalysts. *J. Catal.* **2010**, *273*, 236−244.
(6) Olah, G. A.; Doggweiler, H.; Felberg, J. D.; Frohlich, S.; Grdina, M. J.; Karpeles, R.; Keumi, T.; Inaba, S.-i.; Ip, W. M.; Lammertsma, K.; et al. Onium Ylide chemistry. 1. Bifunctional acid-base-catalyzed conversion of heterosubstituted methanes into ethylene and derived hydrocarbons. The onium ylide mechanism of the C1 .fwdarw. C2 conversion. *J. Am. Chem. Soc.* **1984**, *106*, 2143−2149.
(7) Rousseau, R.; Dixon, D. A.; Kay, B. D.; Dohnálek, Z. Dehydration, dehydrogenation, and condensation of alcohols on supported oxide catalysts based on cyclic (WO3)3 and (MoO3)3 clusters. *Chem. Soc. Rev.* **2014**, *43*, 7664−7680.
(8) Wang, H.; Wu, Y.; Liu, Z.; He, L.; Yao, Z.; Zhao, W. Deposition of WO 3 on Al 2 O 3 via a microwave hydrothermal method to prepare highly dispersed W/Al 2 O 3 hydrodesulfurization catalyst. *Fuel* **2014**, *136*, 185−193.
(9) Schalkwyk, C.; Spamer, A.; Moodley, D. J.; Dube, T.; Reynhardt, J.; Botha, J. M. Application of a WO3/SiO2 catalyst in an industrial environment: part I. *Appl. Catal. Gen.* **2003**, *255*, 121−131.
(10) Wang, Y.; Chen, Q.; Yang, W.; Xie, Z.; Xu, W.; Huang, D. Effect of support nature on WO3/SiO2 structure and butene-1 metathesis. *Appl. Catal. a-General* **2003**, *250*, 25−37.
(11) Mougel, V.; Chan, K.-W.; Siddiqi, G.; Kawakita, K.; Nagae, H.; Tsurugi, H.; Mashima, K.; Safonova, O.; Copéret, C. Low Temperature Activation of Supported Metathesis Catalysts by Organosilicon Reducing Agents. *ACS Cent. Sci.* **2016**, *2*, 569−576.
(12) Can, F.; Courtois, X.; Berland, S.; Seneque, M.; Royer, S.; Duprez, D. Composition dependent performance of alumina-based oxide supported WO3 catalysts for the NH3-SCR reaction and the NSR+SCR coupled process. *Catal. Today* **2015**, *257*, 41−50.
(13) Barrault, J.; Boulinguiez, M.; Forquy, C.; Maurel, R. Synthesis of methyl mercaptan from carbon oxides and H2S with tungsten-alumina catalysts. *Appl. Catal.* **1987**, *33*, 309−330.
(14) Cao, Y.; Wang, J.; Kang, M.; Zhu, Y. Catalytic conversion of glucose and cellobiose to ethylene glycol over Ni-WO3/SBA-15 catalysts. *RSC Adv.* **2015**, *5*, 90904−90912.
(15) Pashigreva, A. V.; Kondratieva, E.; Bermejo-Deval, R.; Gutiérrez, O. Y.; Lercher, J. A. Methanol thiolation over Al 2 O 3 and WS 2 catalysts modified with cesium. *J. Catal.* **2017**, *345*, 308−318.
(16) Mashkina, A. V. Heterogeneous catalytic synthesis of alkanethiols and dialkyl sulfides from alcohols and hydrogen sulfide. *Russ. Chem. Rev.* **1995**, *64*, 1131−1147.
(17) Zhang, Y.; Chen, S.; Wu, M.; Fang, W.; Yang, Y. Promoting effect of SiO2 on the K2WO4/Al2O3 catalysts for methanethiol synthesis from methanol and H2S. *Catal. Commun.* **2012**, *22*, 48−51.
(18) Wang, W.; Li, Y.; Zhang, X.; Fang, W.; Yang, Y. Catalytic synthesis of methanethiol from methanol and carbon disulfide over KW/Al2O3 catalysts. *Catal. Commun.* **2015**, *69*, 104−108.
(19) Zhu, M.; Li, B.; Jehng, J.-M.; Sharma, L.; Taborda, J.; Zhang, L.; Stach, E.; Wachs, I. E.; Wu, Z.; Baltrusaitis, J. Molecular structure and sour gas surface chemistry of supported K 2 O/WO 3 /Al 2 O 3 catalysts. *Appl. Catal., B* **2018**, *232*, 146−154.
(20) Taifan, W.; Baltrusaitis, J. Minireview: direct catalytic conversion of sour natural gas (CH4 + H2S + CO2) components to high value chemicals and fuels. *Catal. Sci. Technol.* **2017**, *7*, 2919−2929.
(21) Ross-Medgaarden, E. I.; Wachs, I. E. Structural Determination of Bulk and Surface Tungsten Oxides with UV−vis Diffuse Reflectance Spectroscopy and Raman Spectroscopy. *J. Phys. Chem. C* **2007**, *111*, 15089−15099.
(22) Soled, S.; Murrell, L. L.; Wachs, I. E.; McVicker, G. B.; Sherman, L. G.; Chan, S.; Dispenziere, N. C.; Baker, R. T. K. Solid State Chemistry of Tungsten Oxide Supported on Alumina. *Solid State Chemistry in Catalysis*; ACS Symposium Series; American Chemical Society, 1985; Vol. *279*, pp 165−182.
(23) Barton, D. G.; Shtein, M.; Wilson, R. D.; Soled, S. L.; Iglesia, E. Structure and Electronic Properties of Solid Acids Based on Tungsten Oxide Nanostructures. *J. Phys. Chem. B* **1999**, *103*, 630−640.
(24) Engweiler, J.; Harf, J.; Baiker, A. WOx/TiO2Catalysts Prepared by Grafting of Tungsten Alkoxides: Morphological Properties and Catalytic Behavior in the Selective Reduction of NO by NH3. *J. Catal.* **1996**, *159*, 259−269.
(25) Wachs, I. E. Raman and IR studies of surface metal oxide species on oxide supports: Supported metal oxide catalysts. *Catal. Today* **1996**, *27*, 437−455.
(26) Rossmedgaarden, E.; Knowles, W.; Kim, T.; Wong, M.; Zhou, W.; Kiely, C.; Wachs, I. New insights into the nature of the acidic catalytic active sites present in ZrO2-supported tungsten oxide catalysts. *J. Catal.* **2008**, *256*, 108−125.
(27) Grant, J. T.; Carrero, C. A.; Love, A. M.; Verel, R.; Hermans, I. Enhanced Two-Dimensional Dispersion of Group v Metal Oxides on Silica. *ACS Catal.* **2015**, *5*, 5787−5793.
(28) Wachs, I. E. Recent conceptual advances in the catalysis science of mixed metal oxide catalytic materials. *Catal. Today* **2005**, *100*, 79−94.
(29) Tittarelli, P.; Iannibello, A.; Villa, P. L. Phase transitions and surface stability of the WO3-γ-Al2O3 system. *J. Solid State Chem.* **1981**, *37*, 95−102.
(30) Kim, T.; Burrows, A.; Kiely, C.; Wachs, I. Molecular/electronic structure-surface acidity relationships of model-supported tungsten oxide catalysts. *J. Catal.* **2007**, *246*, 370−381.
(31) Horsley, J. A.; Wachs, I. E.; Brown, J. M.; Via, G. H.; Hardcastle, F. D. Structure of surface tungsten oxide species in the tungsten trioxide/alumina supported oxide system from x-ray absorption near-edge spectroscopy and Raman spectroscopy. *J. Phys. Chem.* **1987**, *91*, 4014−4020.
(32) Guesmi, H.; Grybos, R.; Handzlik, J.; Tielens, F. Characterization of tungsten monomeric oxide species supported on hydroxylated silica; A DFT study. *RSC Adv.* **2016**, *6*, 39424−39432.
(33) Krokidis, X.; Raybaud, P.; Gobichon, A.-E.; Rebours, B.; Euzen, P.; Toulhoat, H. Theoretical Study of the Dehydration Process of Boehmite to γ-Alumina. *J. Phys. Chem. B* **2001**, *105*, 5121−5130.
(34) Digne, M.; Sautet, P.; Raybaud, P.; Toulhoat, H.; Artacho, E. Structure and stability of aluminum hydroxides: A theoretical study. *J. Phys. Chem. B* **2002**, *106*, 5155−5162.
(35) Raybaud, P.; Digne, M.; Iftimie, R.; Wellens, W.; Euzen, P.; Toulhoat, H. Morphology and Surface Properties of Boehmite (γ-AlOOH): A Density Functional Theory Study. *J. Catal.* **2001**, *201*, 236−246.
(36) Digne, M.; Sautet, P.; Raybaud, P.; Euzen, P.; Toulhoat, H. Hydroxyl Groups on γ-Alumina Surfaces: A DFT Study. *J. Catal.* **2002**, *211*, 1−5.
(37) McBriarty, M. E.; Campbell, G. P.; Drake, T. L.; Elam, J. W.; Stair, P. C.; Ellis, D. E.; Bedzyk, M. J. Atomic-Scale View of VOX-WOX Coreduction on the α-Al2O3 (0001) Surface. *J. Phys. Chem. C* **2015**, *119*, 16179−16187.
(38) McBriarty, M. E.; Ellis, D. E. Cation synergies affect ammonia adsorption over VOX and (V,W)OX dispersed on α-Al2O3 (0001) and α-Fe2O3 (0001). *Surf. Sci.* **2016**, *651*, 41−50.
(39) Kresse, G.; Furthmüller, J. Efficient iterative schemes forab initiototal-energy calculations using a plane-wave basis set. *Phys. Rev. B: Condens. Matter Mater. Phys.* **1996**, *54*, 11169−11186.
(40) Kresse, G.; Joubert, D. From ultrasoft pseudopotentials to the projector augmented-wave method. *Phys. Rev. B: Condens. Matter Mater. Phys.* **1999**, *59*, 1758−1775.
(41) Perdew, J. P.; Wang, Y. Accurate and simple analytic representation of the electron-gas correlation energy. *Phys. Rev. B: Condens. Matter Mater. Phys.* **1992**, *45*, 13244−13249.
(42) Perdew, J. P.; Chevary, J. A.; Vosko, S. H.; Jackson, K. A.; Pederson, M. R.; Singh, D. J.; Fiolhais, C. Atoms, molecules, solids, and surfaces: Applications of the generalized gradient approximation for exchange and correlation. *Phys. Rev. B: Condens. Matter Mater. Phys.* **1992**, *46*, 6671−6687.

DOI: 10.1021/acs.jpcc.8b08214
J. Phys. Chem. C 2018, 122, 24190−24201

(43) Fonari, A.; Stauffer, S. vasp_raman.py. https://github.com/raman-sc/VASP/, 2013.
(44) Digne, M.; Sautet, P.; Raybaud, P.; Euzen, P.; Toulhoat, H. Use of DFT to achieve a rational understanding of acid?basic properties of ?-alumina surfaces. *J. Catal.* **2004**, *226*, 54−68.
(45) Lwin, S.; Keturakis, C.; Handzlik, J.; Sautet, P.; Li, Y.; Frenkel, A. I.; Wachs, I. E. Surface ReOx Sites on Al2O3 and Their Molecular Structure-Reactivity Relationships for Olefin Metathesis. *ACS Catal.* **2015**, *5*, 1432−1444.
(46) Wischert, R.; Copéret, C.; Delbecq, F.; Sautet, P. Revisiting the Structure of Methyltrioxorhenium Chemisorbed on Alumina. *ChemCatChem* **2010**, *2*, 812−815.
(47) Kim, D. S.; Ostromecki, M.; Wachs, I. E. Surface structures of supported tungsten oxide catalysts under dehydrated conditions. *J. Mol. Catal. A: Chem.* **1996**, *106*, 93−102.
(48) Williams, C. C.; Ekerdt, J. G.; Jehng, J. M.; Hardcastle, F. D.; Wachs, I. E. A Raman and Ultraviolet Diffuse Reflectance Spectroscopic Investigation of Alumina-Supported Molybdenum Oxide. *J. Phys. Chem.* **1991**, *95*, 8791−8797.
(49) Daniel, B. A.; Wim, K.; Martin, J. M. L. Assessment of various density functionals and basis sets for the calculation of molecular anharmonic force fields. *Int. J. Quantum Chem.* **2005**, *104*, 830−845.
(50) Peri, J. B. Infrared Study of Adsorption of Ammonia on Dry γ-Alumina1. *J. Phys. Chem.* **1965**, *69*, 231−239.
(51) Medema, J.; Van Bokhoven, J. J. G. M.; Kuiper, A. E. T. Adsorption of Bases on γ-Al2O3. *J. Catal.* **1972**, *25*, 238−244.
(52) Sobalik, Z.; Kozlovwski, R.; Haber, J. Structure of monolayer vanadia $gamma;-alumina catalysts as revealed by IR spectra of probe molecules. *J. Catal.* **1991**, *127*, 665−674.
(53) Jiménez, I.; Centeno, M. A.; Scotti, R.; Morazzoni, F.; Cornet, A.; Morante, J. R. NH[sub 3] Interaction with Catalytically Modified Nano-WO[sub 3] Powders for Gas Sensing Applications. *J. Electrochem. Soc.* **2003**, *150*, H72.
(54) Towns, J.; Cockerill, T.; Dahan, M.; Foster, I.; Gaither, K.; Grimshaw, A.; Hazlewood, V.; Lathrop, S.; Lifka, D.; Peterson, G. D.; et al. XSEDE: Accelerating Scientific Discovery. *Comput. Sci. Eng.* **2014**, *16*, 62−74.

DOI: 10.1021/acs.jpcc.8b08214
J. Phys. Chem. C 2018, 122, 24190−24201